Editors' Suggestion

Experimental Characterization of a Spin Quantum Heat Engine

John P. S. Peterson,[1,†] Tiago B. Batalhão,[2,3,4,†] Marcela Herrera,[2,†] Alexandre M. Souza,[5] Roberto S. Sarthour,[5] Ivan S. Oliveira,[5] and Roberto M. Serra[2,*]

[1]*Institute for Quantum Computing and Department of Physics and Astronomy, University of Waterloo, Waterloo N2L 3G1, Ontario, Canada*

[2]*Centro de Ciências Naturais e Humanas, Universidade Federal do ABC, Avenida dos Estados 5001, 09210-580 Santo André, São Paulo, Brazil*

[3]*Singapore University of Technology and Design, 8 Somapah Road, Singapore 487372, Singapore*

[4]*Centre for Quantum Technologies, National University of Singapore, 3 Science Drive 2, Singapore 117543, Singapore*

将碳-13为中心的三氯甲烷放置在500MHz的核磁共振仪中，在常温常压下得到了近乎完美的奥图循环热机。其概念验证实验中表现出的做功效率达到了42%，距离理论上限的44%，仅差2个百分点。

这个超级微小的热机一共只由5个原子组成，中心是1个碳-13原子，周围是1个氢原子和3个氯原子。其工作原理主要是利用一种被称为Larmor进动的量子效应，确切的说就是碳原子的自旋磁矩，在碳氢键上不同位置所表现出的不同Larmor进动。

在靠近氢原子的位置，进动频率较高；而靠近碳原子的地方，进动频率较低。这种区别，使碳原子自旋的能级宽度有所不同。也就是说，在碳氢键的两端存在能量落差。根据三级模型所指明的原理，就可以产生奥图循环。

这个微小的热机之所以能够在常温常压下工作，主要是因为向外做功过程的弛豫时间非常短，非平衡态的持续时间约为10-4秒，远远小于退相干所需要的秒级时间。所以热机在整个向外做功的过程中，一直可以保持住自己非对角化的哈密顿量，不必担心受到来自环境的噪声侵扰。

Quantum thermal machines perform a thermodynamic cycle employing quantum systems as the working medium. This notion was introduced long ago when Scovil and Schulz-Dubois recognized a three-level maser as a kind of heat engine [1], and since then many theoretical proposals for thermodynamical cycles at the quantum scale have been discussed [2–32]. Microscopic quantum heat engines may operate at a scale where both thermal and quantum fluctuations are relevant. The thermodynamic description of such devices operating at finite time should also include the inherent nondeterministic nature of the quantum evolution and nonequilibrium features. In this context, quantities as work, heat, and entropy production are associated with statistical distributions that satisfy fluctuation theorems [33–35] for a thermodynamical cycle [36,37].

The enthusiastic interest in quantum thermal machines has grown with the possibility of controlling nonequilibrium dynamics of microscopic systems, achievable in platforms such as trapped ions [38,39], quantum dots [40–42], single electron boxes [43], optomechanical oscillators [44–47], etc. Some experimental success related to the implementation of microscale heat engines has been reported in a context where quantum coherence effects are not prominent (which can be regarded as a classical context) [48–53]. Recently, a single trapped ion was employed as a working medium to perform a thermodynamic cycle [54]. Despite the latter implementation being based on a single quantum system, the operating temperatures are such that the thermal energy is considerably higher than the energy level separation of the magnetic trap. As a consequence, effects of quantum fluctuations are dwarfed by thermal fluctuations, allowing a classical description.

The full characterization of a finite-time operation of a quantum heat engine may also be associated with the assessment of the probability distribution of energy fluctuations, which can take the form of work or heat flow [55]. This assessment embodies significant experimental challenges that have remained elusive up to now.

In this contribution, we used a nuclear magnetic resonance (NMR) setup [56] to implement and characterize a quantum version of the Otto cycle [4]. As a proof-of-concept implementation of a quantum heat engine operating at finite time, we employed a ^{13}C-labeled $CHCl_3$ liquid sample diluted in Acetone-D6 and a 500 MHz Varian NMR spectrometer. The spin 1/2 of the ^{13}C nucleus is the working medium, whereas the ^{1}H nuclear spin will be used as a heat bus. High radio-frequency (rf) modes near the hydrogen Larmor frequency play the role of the hot environment, while low rf modes near to carbon resonance frequency plays the role of the cold environment. Chlorine isotopes' nuclei provide mild environmental effects. An interferometric method [57–61] is applied to assess energy fluctuations to characterize the work and heat statistics

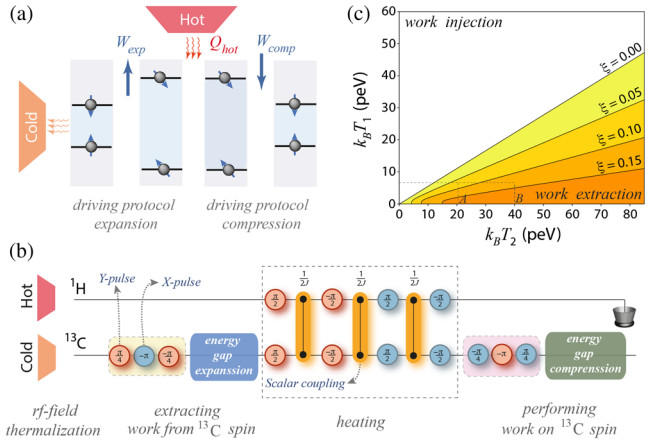

FIG. 1. Quantum heat engine schematics. (a) Thermodynamic cycle employing a spin 1/2 as the working medium. (b) Simplified pulse sequence of the experimental protocol. ^{1}H and ^{13}C nuclear spins are initially prepared in thermal states corresponding to hot and cold spin temperatures, respectively. Blue (red) circles represent x (y) rotations by the displayed angle produced by transverse rf pulses. Orange connections stand for free evolutions under the scalar interaction ($\mathcal{H}_J$) during the time displayed above the symbol. The unitary driving for the energy gap expansion (compression) protocol is implemented by a time-modulated rf field resonant with the ^{13}C nuclear spin. The hydrogen nucleus is used to deliver the heat at the proper part of the cycle, working as a heat bus. (c) Required temperatures for work extraction at finite-time operation mode. The engine extracts work only if the hot (T_2) and cold (T_1) source temperatures correspond to a point below the curve defined by the energy level transition probability ξ.

as well as the irreversibility aspects of this spin engine. The operation regime is such that the typical thermal energy scale is of the same order of the typical separation of the quantum energy levels, turning the effects of quantum fluctuations as important as the ones from thermal fluctuations. We have also experimentally endorsed an expression for the efficiency lag related to the entropy production that hinders the implemented engine to attain the Carnot efficiency at finite time. The cycle was established at different finite-time regimes, ranging from a very irreversible one to one of almost maximum efficiency, allowing for the identification of the maximum power operation.

The quantum version of the Otto cycle [4,20] consists of a four-stroke protocol as illustrated in Fig. 1(a).

Cooling stroke.—Using spatial average techniques employed by rf and gradient fields, the ^{13}C nuclear spin is initially chilled to a pseudothermal state, equivalent to $\rho_0^{\mathrm{eq},1} = e^{-\beta_1 \mathcal{H}_1^{\mathrm{C}}}/Z_1$ [62,63], at a cold inverse spin temperature $\beta_1 = (k_B T_1)^{-1}$, where $Z_1 = \mathrm{tr}(e^{-\beta_1 \mathcal{H}_1^{\mathrm{C}}})$ is the partition function, k_B is the Boltzmann constant, T_1 is the absolute spin temperature of the cold reference state, and the Hamiltonian $\mathcal{H}_1^{\mathrm{C}}$ will be defined later.

Expansion stroke.—The working medium Hamiltonian is driven by a time-modulated rf field resonant with the ^{13}C nuclear spin. Initially it can be described by $\mathcal{H}_1^{\mathrm{C}} = -h\nu_1 \sigma_x^{\mathrm{C}}/2$ (with the rf-field intensity adjusted such that $\nu_1 = 2.0$ kHz, and $\sigma_{x,y,z}^{\mathrm{C}}$ being the Pauli spin operators for ^{13}C nuclear spin), in a rotating frame at the ^{13}C Larmor frequency ($\approx$125 MHz). From $t = 0$ up to $t = \tau$, the system Hamiltonian is driven according to $\mathcal{H}_{\mathrm{exp}}^{\mathrm{C}}(t) = -\frac{1}{2} h\nu(t)$ $[\cos(\pi t/2\tau)\sigma_x^{\mathrm{C}} + \sin(\pi t/2\tau)\sigma_y^{\mathrm{C}}]$, expanding (exp) the nuclear spin energy gap linearly as $\nu(t) = \nu_1[1 - (t/\tau)] + \nu_2(t/\tau)$ (with $\nu_2 = 3.6$ kHz and $t \in [0, \tau]$). The energy gap expansion happens in a driving time length, τ, that will be varied in different experiments between 100 and 700 μs. The driving time length ($\propto 10^{-4}$ s) is much shorter than the typical decoherence timescales, which are on the order of seconds. In this way, we can describe this process by a unitary evolution, $\mathcal{U}_\tau$ [59,61,63], that drives the ^{13}C nuclear spin to an out-of-equilibrium state (ρ_τ^{C}), which is, in general, not diagonal in the energy eigenbasis of the final Hamiltonian of the expansion protocol, $\mathcal{H}_2^{\mathrm{C}} = \mathcal{H}_{\mathrm{exp}}^{\mathrm{C}}(\tau) = -h\nu_1 \sigma_y^{\mathrm{C}}/2$.

Heating stroke.—The working medium (^{13}C nucleus) exchanges heat with the ^{1}H nuclear spin, which was initially prepared at a higher temperature [62,63] than the ^{13}C nuclear spin, reaching full thermalization at the hot inverse spin temperature $\beta_2 = (k_B T_2)^{-1}$. The full thermalization process is effectively implemented by a sequence of free evolutions under the scalar interaction, $\mathcal{H}_J = (\pi\hbar/2) J \sigma_z^{\mathrm{H}} \sigma_z^{\mathrm{C}}$ (with $J \approx 215.1$ Hz), between both nuclei and rf pulses to produce suitable rotations as sketched in Fig. 1(b). After thermalization, the state of the ^{13}C nuclei is the hot equilibrium state, equivalent to $\rho_0^{\mathrm{eq},2} = e^{-\beta_2 \mathcal{H}_2^{\mathrm{C}}}/Z_2$.

Compression stroke.—Subsequently, an energy gap compression is performed, according to the time-reversed process [64] of the expansion protocol; i.e., the Hamiltonian is driven in a way that $\mathcal{H}_{\mathrm{comp}}^{\mathrm{C}}(t) = -\mathcal{H}_{\mathrm{exp}}^{\mathrm{C}}(\tau - t)$.

Many cycles of this proof-of-concept experiment can be performed by repeating successively the pulse sequence protocol described in Fig. 1(b). It is interesting to note that each experimental run involves spatial averages on a diluted liquid sample containing about 10^{17} molecules, which can be regarded as noninteracting with each other due to the sample dilution. Each experimental result for the quantities of interest represents an average over many copies of a single molecular spin engine.

The finite-time (expansion and compression) driven processes are associated with transitions among the instantaneous eigenstates of the working medium Hamiltonian (see Fig. S3 in the Supplemental Material [63]), resulting in entropy production [61,65], which is the main source of irreversibility in the implemented cycle. In this way, quantum coherence also contributes to the irreversibility [66–68].

Considering the aforementioned description of the finite-time thermodynamical cycle, we can write the average values of the extracted work (W_{eng}) from the engine and the absorbed heat (Q_{hot}) from the ^{1}H nuclear spin as

$$\langle W_{\rm eng}\rangle = \frac{h}{2}(\nu_2-\nu_1)[\tanh(\beta_1 h\nu_1)-\tanh(\beta_2 h\nu_2)] - h\xi[\nu_1\tanh(\beta_2 h\nu_2)+\nu_2\tanh(\beta_1 h\nu_1)], \quad (1)$$

$$\langle Q_{\rm hot}\rangle = \frac{h}{2}\nu_2[\tanh(\beta_1 h\nu_1)-\tanh(\beta_2 h\nu_2)] - \xi h\nu_2\tanh(\beta_1 h\nu_1), \quad (2)$$

where $\xi = |\langle\Psi^2_\pm|\mathcal{U}_\tau|\Psi^1_\mp\rangle|^2 = |\langle\Psi^1_\pm|\mathcal{V}_\tau|\Psi^2_\mp\rangle|^2$ are the transition probabilities between the instantaneous eigenstates $|\Psi^1_\pm\rangle$ ($|\Psi^2_\pm\rangle$) of the Hamiltonian $\mathcal{H}^{\rm C}_1$ ($\mathcal{H}^{\rm C}_2$), and $\mathcal{V}_\tau$ is the unitary evolution describing the compression protocol, satisfying $\mathcal{V}_\tau = \mathcal{U}^\dagger_\tau$. The nuclear spin system operates as a heat engine when $\langle W_{\rm eng}\rangle > 0$, otherwise work is being injected in the device during the cycle. Two conditions must be met to allow work extraction. The first is the requirement that $(\nu_2-\nu_1)[\tanh(\beta_1 h\nu_1)-\tanh(\beta_2 h\nu_2)] \geq 0$, which is equivalent to the classical-scenario bound, $1 \leq \nu_2/\nu_1 \leq T_2/T_1$. The second condition imposes a limit on the admitted transition probability among the energy levels which reads

$$\xi \leq \frac{(\nu_2-\nu_1)[\tanh(\beta_1 h\nu_1)-\tanh(\beta_2 h\nu_2)]}{2[\nu_1\tanh(\beta_2 h\nu_2)+\nu_2\tanh(\beta_1 h\nu_1)]}. \quad (3)$$

This condition, illustrated in Fig. 1(c), is related to the rapidity of the energy gap expansion (compression) protocol and to the fact that the driving Hamiltonian does not commute at different times. For a given protocol (that sets the ξ value) condition (3) depends only on the energy gap compression factor, $r = \nu_2/\nu_1$ ($r \simeq 1.8$ in our experiment). The system operates in the working extraction mode if the point that characterizes the temperature of both heat sources lies below the contour curve in Fig. 1(c) for a given transition probability.

The spin-engine efficiency can also be written in terms of the energy level transition probability as

$$\eta = \frac{\langle W_{\rm eng}\rangle}{\langle Q_{\rm hot}\rangle} = 1 - \frac{\nu_1}{\nu_2}\frac{(1-2\xi\mathcal{F})}{(1-2\xi\mathcal{G})}, \quad (4)$$

where $\mathcal{F} = \tanh(\beta_2 h\nu_2)[\tanh(\beta_1 h\nu_1)-\tanh(\beta_2 h\nu_2)]^{-1}$ and $\mathcal{G} = \mathcal{F}\tanh(\beta_1 h\nu_1)/\tanh(\beta_2 h\nu_2)$. The Otto limit ($\eta_{\rm Otto}$) is recovered in an adiabatic (transitionless, i.e., $\xi = 0$) driving. On the other hand, in the finite-time regime, efficiency (4) decreases as ξ increases. Alternatively, we can derive an expression for the engine efficiency in terms of efficiency lags (associated with entropy production [29–31,61]) as $\eta = \eta_{\rm Carnot} - \mathcal{L}$, and the lag is given by [63]

$$\mathcal{L} = \frac{\mathcal{S}(\mathcal{U}_\tau\rho_0^{\rm eq,1}\mathcal{U}_\tau^\dagger\|\rho_0^{\rm eq,2}) + \mathcal{S}(\mathcal{V}_\tau\rho_0^{\rm eq,2}\mathcal{V}_\tau^\dagger\|\rho_0^{\rm eq,1})}{\beta_1\langle Q_{\rm hot}\rangle}, \quad (5)$$

where $\mathcal{S}(\rho_a\|\rho_b) = {\rm tr}[\rho_a(\ln\rho_a - \ln\rho_b)]$ is the relative entropy and $\eta_{\rm Carnot} = 1 - T_1/T_2$ the standard Carnot efficiency.

Work extracted from (performed on) the ^{13}C nuclear spin during the energy gap expansion (compression) driving protocol is actually a stochastic variable, described by a probability distribution [36,37], $P_{\rm exp}(W)$ [$P_{\rm comp}(W)$]. The full thermalization with the hot source allows us to write the work performed in each Hamiltonian driving stroke of the cycle as independent variables. So the net extracted work from the engine is a convolution of the two marginal work probability distributions, which can be assessed by the interferometric approach [59,61]. In this experiment, the characteristic function of the work probability distribution is measured. In the energy gap expansion stroke, it is given by

$$\chi_{\rm exp}(u) = {\rm tr}[\mathcal{U}_\tau e^{-iu\mathcal{H}^{\rm C}_{\rm exp,0}}\rho_0^{\rm eq,1}(e^{-iu\mathcal{H}^{\rm C}_{\rm exp,\tau}}\mathcal{U}_\tau)^\dagger] = \sum_{n,m=0}^{1} p_n^0 p^\tau_{m|n} e^{iu(\epsilon^\tau_m - \epsilon^0_n)}, \quad (6)$$

where p_n^0 is the occupation probability of the nth energy level in the cold initial thermal state ($\rho_0^{\rm eq,1}$), $p^\tau_{m|n} = \xi + (1-2\xi)\delta_{m,n}$ is the transition probability between the Hamiltonian eigenstates induced by the time-dependent quantum dynamics, and ϵ^τ_m and ϵ^0_n are eigenenergies of the Hamiltonians $\mathcal{H}^{\rm C}_1$ and $\mathcal{H}^{\rm C}_2$, respectively. Analogous expressions hold for the compression stroke [$\chi_{\rm comp}(u)$] [63]. The characteristic function for the engine net extracted work is the product of characteristic functions for both Hamiltonian driving protocols, i.e., $\chi_{\rm eng}(u) = \chi_{\rm comp}(u)\chi_{\rm exp}(u)$. Thus, the inverse Fourier transform of the measured $\chi_{\rm eng}(u)$ provides the work probability distribution for the quantum engine as $P_{\rm eng}(W) = \int du\chi_{\rm eng}(u)e^{iuW}$, and the mean value of the extracted work can be obtained from the statistics as $\langle W_{\rm eng}\rangle = \int dW P_{\rm eng}(W)W$.

We characterized the work distribution in different operation modes of the spin engine, varying the driving time length (τ) and the hot source temperature, with representative results displayed in Fig. 2. The initial spin temperatures of the ^{1}H and ^{13}C nuclei were verified by quantum state tomography (QST) [56], which confirmed the Gibbs state preparation. The spin temperature of the ^{13}C cold initial state is equivalent to $k_B T_1 = (6.6 \pm 0.1)$ peV, while the ^{1}H was prepared in two hot states (A and B) corresponding to $k_B T_2^A = (21.5 \pm 0.4)$ peV and $k_B T_2^B = (40.5 \pm 3.7)$ peV.

There are nine observed peaks in Fig. 2(a), corresponding to the fastest implemented engine driving. A fit of these experimental data allows us to determine the transition probability ξ that vary from $\xi = 0.02 \pm 0.02$ (for $\tau = 700$ μs) to $\xi = 0.38 \pm 0.04$ (for $\tau = 100$ μs). We observe that when the Hamiltonian driving is slower, as in Fig. 2(b), some of the work distribution peaks get decreased to the point of being barely noticeable amid the noise (associated with the Fourier analysis) since the dynamics is getting

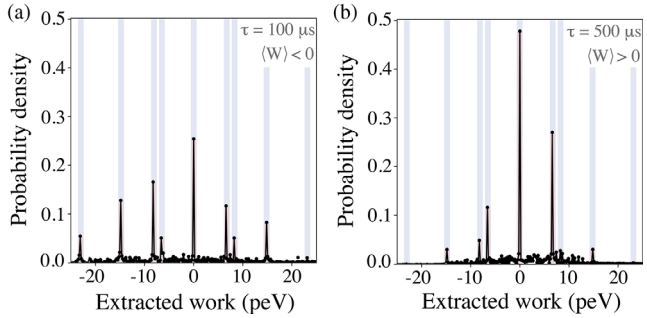

FIG. 2. Extracted work probability distribution of the quantum engine with Hamiltonian driving time lengths (a) $\tau = 100$ μs and (b) $\tau = 500$ μs. Cold and hot source temperatures are set at $k_B T_1 = (6.6 \pm 0.1)$ peV and $k_B T_2^B = (40.5 \pm 3.7)$ peV, respectively. The experimental data (points) are well fitted by a sum of nine Lorentzian peaks (the solid line) centered approximately at $0, \pm h(\nu_2 - \nu_1), \pm\nu_1, \pm\nu_2$, and $\pm h(\nu_2 + \nu_1)$ (dashed columns), in agreement with the theoretical expectation (see Fig. S3 in the Supplemental Material [63]). The error bars are smaller than the symbol size and are not shown.

closer to the adiabatic one. We also characterize the Hamiltonian driving protocol by means of quantum process tomography [69,70] to certify that it implements an almost unitary process [63].

The absorbed heat from the hot source (^{1}H nuclear spin) is also a stochastic variable and its probability distribution, $\mathcal{P}(Q)$, could be assessed by a two-time energy measurement scheme [71]. However, in a full thermalization process, the measurement of energy at the end of the process is uncorrelated with the measurement at the start. Then, two QSTs are enough to provide a direct evaluation of the heat probability distribution in this implementation [63]. One of them is done at the end of the energy gap expansion stroke (where the state is typically out of equilibrium), while the other is done at the start of the energy gap compression stroke (and thus should result in the hot thermal state). So the mean heat from the hot source can be expressed as $\langle Q_{\rm hot}\rangle = \int dQ\mathcal{P}(Q)Q$.

With the aforementioned data, we have fully characterized the quantum heat engine. Its performance can be rated according to the average work extracted per cycle, efficiency, efficiency lag, and the average delivered power. These figures of merit are shown in Figs. 3(a)–3(d). The work extraction regime requires a lower bound on the driving time length, as can be seen in Fig. 3(a), and also was anticipated by condition (3). If the engine is operated at a too-fast driving time length τ (smaller than $\approx$200 μs in this case), the entropy production is so large that it is not possible to extract work. This entropy production decreases with a slower operation rate, although not monotonically. The latter fact is a consequence of the specific form of the Hamiltonian time modulation employed in our implementation and does not generalize to other drivings.

Figure 3(b) illustrates the fact that slower operation leads to better efficiency. Nonetheless, the quantum engine irreversibility can also be characterized by the efficiency lag (5) measured by QST at different strokes. We observe a complete agreement between the lag displayed in Fig. 3(c) and the efficiency measured as the mean work and heat ratio [Fig. 3(b)]. For the implemented quantum cycle, the main source of irreversibility is the divergence (accounted for by the relative entropy) of the state achieved after the Hamiltonian driving protocols (expansion and compression) and the reference (hot and cold) thermal states.

We are often interested in power, and a too-slow engine operation, as in adiabatic dynamics, cannot deliver a fairly good amount of power. Extracted power is maximized when the energy gap expansion (compression) protocol takes about 310 μs, as can be noted in Fig. 3(d). Quicker protocols are worse due to considerable entropy production associated with energy level transitions during the dynamics [Fig. 3(c)], while slower driven protocols are also worse since they take more time to deliver a similar amount of work [Fig. 3(a)]. The effective full thermalization with the hot source (^{1}H nucleus) employed in our experiment [the central part of the pulse sequence in Fig. 1(b)] lasts for about 7 ms, and it takes the same time length in all operation modes of the spin engine. In this fashion, we have opted to describe all results in terms of the expansion and compression Hamiltonian driving time length τ, which is the finite-time feature in this spin-engine implementation.

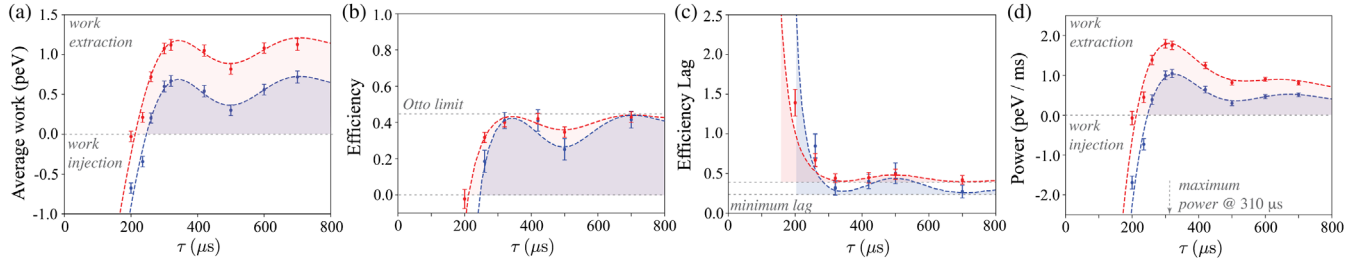

FIG. 3. Spin quantum engine figures of merit: (a) average extracted work, (b) efficiency, (c) efficiency lag due to entropy production [according Eq. (5); the minimum lag is $\eta_{\rm Carnot} - \eta_{\rm Otto}$], and (d) extracted power as a function of the driving protocol time length (τ). Points represent experimental data. The dashed lines are based on theoretical predictions and numerical simulations. In all experiments, the spin temperature of the cold source is set at $k_B T_1 = (6.6 \pm 0.1)$ peV. Data in blue and red correspond to implementations with the hot source spin temperatures set at $k_B T_2^A = (21.5 \pm 0.4)$ peV and $k_B T_2^B = (40.5 \pm 3.7)$ peV, respectively.

We performed an experimental proof of concept of a quantum heat engine based on a nuclear spin where the typical energy gaps, about 8.27 peV, are of the order of heat source energy, $k_B(T_2 - T_1)$ ($\approx$15 peV). The extracted work per cycle may be on the same order of magnitude (a few peV) depending on the driving protocol. At maximum power ($\tau \approx 310$ μs), the engine efficiency, $\eta = 42 \pm 6\%$, is very close to the Otto limit, $\eta_{\mathrm{Otto}} = 44\%$, for the compression factor employed in this implementation. The power delivered by the quantum engine, in the finite-time operation mode, is ultimately limited by quantum fluctuations (transitions among the instantaneous energy eigenstates), which are also related to entropy production [61,65] leading to a "quantum friction" [29,30]. Assessing the statistics of energy fluctuations in the implemented engine, we fully characterize its irreversibility and efficiency lag. The investigation of this data can also allow the quantum engine optimization by choosing optimal driving protocols. The methods employed here to assess energy fluctuations and to characterize irreversibility in the quantum engine are versatile and can be applied to other experimental settings. The developed spin-engine architecture is a comprehensive platform for future investigations of thermodynamical cycles at microscale, which would involve, for instance, nonequilibrium, nonclassical, and correlated heat sources, allowing for the detailed study of a plethora of effects in quantum thermodynamics [23,24].

We thank E. Lutz, M. Paternostro, L. C. Céleri, C. I. Henao, P. A. Camati, K. Micadei, and F. L. Semião for the valuable discussions. We acknowledge financial support from Fundação Universidade Federal do ABC (UFABC), CNPq, CAPES, FAPERJ, and FAPESP. J. P. S. P. thanks Innovation, Science and Economic Development Canada, the Government of Ontario, and CIFAR for the support. T. B. B. acknowledges support from National Research Foundation (Singapore), Ministry of Education (Singapore), and the U.S. Air Force Office of Scientific Research (Grant No. FA2386-15-1-4082). R. M. S. gratefully acknowledges financial support from the Royal Society through the Newton Advanced Fellowship scheme (Grant No. NA140436) and the Multiuser Central Facilities of UFABC for the technical support. This research was performed as part of the Brazilian National Institute of Science and Technology for Quantum Information (INCT-IQ).

*serra@ufabc.edu.br
†These authors contributed equally to this work.

[1] H. E. D. Scovil and E. O. Schulz-DuBois, Three-Level Masers as Heat Engines, Phys. Rev. Lett. **2**, 262 (1959).
[2] R. Alicki, The quantum open system as a model of the heat engine, J. Phys. A **12**, L103 (1979).
[3] E. Geva and R. Kosloff, A quantum-mechanical heat engine operating in finite time. A model consisting of spin- 1/2 systems as the working fluid, J. Chem. Phys. **96**, 3054 (1992).
[4] T. D. Kieu, The Second Law, Maxwell's Demon, and Work Derivable from Quantum Heat Engines, Phys. Rev. Lett. **93**, 140403 (2004).
[5] H. T. Quan, Y. Xi Liu, C. P. Sun, and F. Nori, Quantum thermodynamic cycles and quantum heat engines, Phys. Rev. E **76**, 031105 (2007).
[6] P. Hänggi and F. Marchesoni, Artificial Brownian motors: Controlling transport on the nanoscale, Rev. Mod. Phys. **81**, 387 (2009).
[7] N. Linden, S. Popescu, and P. Skrzypczyk, How Small Can Thermal Machines Be? The Smallest Possible Refrigerator, Phys. Rev. Lett. **105**, 130401 (2010).
[8] L. A. Correa, J. P. Palao, D. Alonso, and G. Adesso, Quantum-enhanced absorption refrigerators, Sci. Rep. **4**, 3949 (2014).
[9] J. P. Palao, L. A. Correa, G. Adesso, and D. Alonso, Efficiency of inefficient endoreversible thermal machines, Braz. J. Phys. **46**, 282 (2016).
[10] R. Uzdin and R. Kosloff, The multilevel four-stroke swap engine and its environment, New J. Phys. **16**, 095003 (2014).
[11] R. Uzdin, A. Levy, and R. Kosloff, Equivalence of Quantum Heat Machines, and Quantum-Thermodynamic Signatures, Phys. Rev. X **5**, 031044 (2015).
[12] F. C. Binder, S. Vinjanampathy, K. Modi, and J. Goold, Quantacell: Powerful charging of quantum batteries, New J. Phys. **17**, 075015 (2015).
[13] D. Gelbwaser-Klimovsky, R. Alicki, and G. Kurizki, Minimal universal quantum heat machine, Phys. Rev. E **87**, 012140 (2013).
[14] M. O. Scully, M. S. Zubairy, G. S. Agarwal, and H. Walther, Extracting work from a single heat bath via vanishing quantum coherence, Science **299**, 862 (2003).
[15] N. Brunner, N. Linden, S. Popescu, and P. Skrzypczyk, Virtual qubits, virtual temperatures, and the foundations of thermodynamics, Phys. Rev. E **85**, 051117 (2012).
[16] R. Gallego, A. Riera, and J. Eisert, Thermal machines beyond the weak coupling regime, New J. Phys. **16**, 125009 (2014).
[17] R. Kosloff and A. Levy, Quantum heat engines and refrigerators: Continuous devices, Annu. Rev. Phys. Chem. **65**, 365 (2014).
[18] A. Mari, A. Farace, and V. Giovannetti, Quantum optomechanical piston engines powered by heat, J. Phys. B **48**, 175501 (2015).
[19] N. Killoran, S. F. Huelga, and M. B. Plenio, Enhancing light-harvesting power with coherent vibrational interactions: A quantum heat engine picture, J. Chem. Phys. **143**, 155102 (2015).
[20] A. Alecce, F. Galve, N. Lo Gullo, L. Dell'Anna, F. Plastina, and R. Zambrini, Quantum Otto cycle with inner friction: Finite-time and disorder effects, New J. Phys. **17**, 075007 (2015).
[21] P. P. Hofer, M. Perarnau-Llobet, J. B. Brask, R. Silva, M. Huber, and N. Brunner, Autonomous quantum refrigerator in a circuit-QED architecture based on a Josephson junction, Phys. Rev. B **94**, 235420 (2016).
[22] M. Campisi and R. Fazio, The power of a critical heat engine, Nat. Commun. **7**, 11895 (2016).

[23] J. Goold, M. Huber, A. Riera, L. del Rio, and P. Skrzypczyk, The role of quantum information in thermodynamics—A topical review, J. Phys. A **49**, 143001 (2016).
[24] S. Vinjanampathy and J. Anders, Quantum thermodynamics, Contemp. Phys. **57**, 545 (2016).
[25] C. Elouard, D. Herrera-Martí, B. Huard, and A. Auffèves, Extracting Work from Quantum Measurement in Maxwell Demon Engines, Phys. Rev. Lett. **118**, 260603 (2017).
[26] A. Dechant, N. Kiesel, and E. Lutz, All-Optical Nanomechanical Heat Engine, Phys. Rev. Lett. **114**, 183602 (2015).
[27] G. Watanabe, B. P. Venkatesh, P. Talkner, and A. del Campo, Quantum Performance of Thermal Machines over Many Cycles, Phys. Rev. Lett. **118**, 050601 (2017).
[28] B. Reid, S. Pigeon, M. Antezza, and G. De Chiara, A self-contained quantum harmonic engine, Europhys. Lett. **120**, 60006 (2018).
[29] T. Feldmann and R. Kosloff, Quantum four-stroke heat engine: Thermodynamic observables in a model with intrinsic friction, Phys. Rev. E **68**, 016101 (2003).
[30] F. Plastina, A. Alecce, T. J. G. Apollaro, G. Falcone, G. Francica, F. Galve, N. Lo Gullo, and R. Zambrini, Irreversible Work and Inner Friction in Quantum Thermodynamic Processes, Phys. Rev. Lett. **113**, 260601 (2014).
[31] N. Shiraishi and H. Tajima, Efficiency versus speed in quantum heat engines: Rigorous constraint from Lieb-Robinson bound, Phys. Rev. E **96**, 022138 (2017).
[32] G. Benenti, G. Casati, K. Saito, and R. S. Whitney, Fundamental aspects of steady-state conversion of heat to work at the nanoscale, Phys. Rep. **694**, 1 (2017).
[33] M. Esposito, U. Harbola, and S. Mukamel, Nonequilibrium fluctuations, fluctuation theorems, and counting statistics in quantum systems, Rev. Mod. Phys. **81**, 1665 (2009).
[34] M. Campisi, P. Hänggi, and P. Talkner, Colloquium: Quantum fluctuation relations: Foundations and applications, Rev. Mod. Phys. **83**, 771 (2011).
[35] P. Hänggi and P. Talkner, The other QFT, Nat. Phys. **11**, 108 (2015).
[36] M. Campisi, Fluctuation relation for quantum heat engines and refrigerators, J. Phys. A **47**, 245001 (2014).
[37] M. Campisi, J. Pekola, and R. Fazio, Non-equilibrium fluctuations in quantum heat engines: Theory, example, and possible solid state experiments, New J. Phys. **17**, 035012 (2015).
[38] O. Abah, J. Roßnagel, G. Jacob, S. Deffner, F. Schmidt-Kaler, K. Singer, and E. Lutz, Single-Ion Heat Engine at Maximum Power, Phys. Rev. Lett. **109**, 203006 (2012).
[39] J. Roßnagel, O. Abah, F. Schmidt-Kaler, K. Singer, and E. Lutz, Nanoscale Heat Engine Beyond the Carnot Limit, Phys. Rev. Lett. **112**, 030602 (2014).
[40] D. M. Kennes, D. Schuricht, and V. Meden, Efficiency and power of a thermoelectric quantum dot device, Europhys. Lett. **102**, 57003 (2013).
[41] R. Sánchez, B. Sothmann, A. N. Jordan, and M. Büttiker, Correlations of heat and charge currents in quantum-dot thermoelectric engines, New J. Phys. **15**, 125001 (2013).
[42] B. Sothmann, R. Sánchez, and A. N. Jordan, Thermoelectric energy harvesting with quantum dots, Nanotechnology **26**, 032001 (2014).
[43] T. L. van den Berg, F. Brange, and P. Samuelsson, Energy and temperature fluctuations in the single electron box, New J. Phys. **17**, 075012 (2015).
[44] K. Zhang, F. Bariani, and P. Meystre, Quantum Optomechanical Heat Engine, Phys. Rev. Lett. **112**, 150602 (2014).
[45] C. Bergenfeldt, P. Samuelsson, B. Sothmann, C. Flindt, and M. Büttiker, Hybrid Microwave-Cavity Heat Engine, Phys. Rev. Lett. **112**, 076803 (2014).
[46] C. Elouard, M. Richard, and A. Auffèves, Reversible work extraction in a hybrid opto-mechanical system, New J. Phys. **17**, 055018 (2015).
[47] M. Brunelli, A. Xuereb, A. Ferraro, G. De Chiara, N. Kiesel, and M. Paternostro, Out-of-equilibrium thermodynamics of quantum optomechanical systems, New J. Phys. **17**, 035016 (2015).
[48] T. Hugel, N. B. Holland, A. Cattani, L. Moroder, M. Seitz, and H. E. Gaub, Single-molecule optomechanical cycle, Science **296**, 1103 (2002).
[49] P. G. Steeneken, K. Le Phan, M. J. Goossens, G. E. J. Koops, G. J. A. M. Brom, C. van der Avoort, and J. T. M. van Beek, Piezoresistive heat engine and refrigerator, Nat. Phys. **7**, 354 (2011).
[50] V. Blickle and C. Bechinger, Realization of a micrometre-sized stochastic heat engine, Nat. Phys. **8**, 143 (2012).
[51] J.-P. Brantut, C. Grenier, J. Meineke, D. Stadler, S. Krinner, C. Kollath, T. Esslinger, and A. Georges, A thermoelectric heat engine with ultracold atoms, Science **342**, 713 (2013).
[52] H. Thierschmann, R. Sánchez, B. Sothmann, F. Arnold, C. Heyn, W. Hansen, H. Buhmann, and L. W. Molenkamp, Three-terminal energy harvester with coupled quantum dots, Nat. Nanotechnol. **10**, 854 (2015).
[53] F. Schmidt, A. Magazzù, A. Callegari, L. Biancofiore, F. Cichos, and G. Volpe, Microscopic Engine Powered by Critical Demixing, Phys. Rev. Lett. **120**, 068004 (2018).
[54] J. Roßnagel, S. T. Dawkins, K. N. Tolazzi, O. Abah, E. Lutz, F. Schmidt-Kaler, and K. Singer, A single-atom heat engine, Science **352**, 325 (2016).
[55] V. Holubec and A. Ryabov, Work and power fluctuations in a critical heat engine, Phys. Rev. E **96**, 030102 (2017).
[56] I. S. Oliveira, T. J. Bonagamba, R. S. Sarthour, J. C. C. Freitas, and E. R. deAzevedo, *NMR Quantum Information Processing* (Elsevier, Amsterdam, 2007).
[57] R. Dorner, S. R. Clark, L. Heaney, R. Fazio, J. Goold, and V. Vedral, Extracting Quantum Work Statistics and Fluctuation Theorems by Single-Qubit Interferometry, Phys. Rev. Lett. **110**, 230601 (2013).
[58] L. Mazzola, G. De Chiara, and M. Paternostro, Measuring the Characteristic Function of the Work Distribution, Phys. Rev. Lett. **110**, 230602 (2013).
[59] T. B. Batalhão, A. M. Souza, L. Mazzola, R. Auccaise, R. S. Sarthour, I. S. Oliveira, J. Goold, G. De Chiara, M. Paternostro, and R. M. Serra, Experimental Reconstruction of Work Distribution and Study of Fluctuation Relations in a Closed Quantum System, Phys. Rev. Lett. **113**, 140601 (2014).
[60] J. Goold, U. Poschinger, and K. Modi, Measuring the heat exchange of a quantum process, Phys. Rev. E **90**, 020101 (2014).
[61] T. B. Batalhão, A. M. Souza, R. S. Sarthour, I. S. Oliveira, M. Paternostro, E. Lutz, and R. M. Serra, Irreversibility and

the Arrow of Time in a Quenched Quantum System, Phys. Rev. Lett. **115**, 190601 (2015).

[62] K. Micadei, J. P. S. Peterson, A. M. Souza, R. S. Sarthour, I. S. Oliveira, G. T. Landi, T. B. Batalhão, R. M. Serra, and E. Lutz, Reversing the direction of heat flow using quantum correlations, Nat. Commun. **10**, 2456 (2019).

[63] See Supplemental Material at http://link.aps.org/supplemental/10.1103/PhysRevLett.123.240601 for details of the experimental and theoretical analysis.

[64] P. A. Camati and R. M. Serra, Verifying detailed fluctuation relations for discrete feedback-controlled quantum dynamics, Phys. Rev. A **97**, 042127 (2018).

[65] P. A. Camati, J. P. S. Peterson, T. B. Batalhão, K. Micadei, A. M. Souza, R. S. Sarthour, I. S. Oliveira, and R. M. Serra, Experimental Rectification of Entropy Production by Maxwell's Demon in a Quantum System, Phys. Rev. Lett. **117**, 240502 (2016).

[66] K. Brandner and U. Seifert, Periodic thermodynamics of open quantum systems, Phys. Rev. E **93**, 062134 (2016).

[67] K. Brandner, M. Bauer, and U. Seifert, Universal Coherence Induced Power Losses of Quantum Heat Engines in Linear Response, Phys. Rev. Lett. **119**, 170602 (2017).

[68] P. A. Camati, J. F. G. Santos, and R. M. Serra, Coherence effects in the performance of the quantum Otto heat engine, Phys. Rev. A **99**, 062103 (2019).

[69] I. L. Chuang and M. A. Nielsen, Prescription for experimental determination of the dynamics of a quantum black box, J. Mod. Opt. **44**, 2455 (1997).

[70] M. A. Nielsen and I. L. Chuang, *Quantum Computation and Quantum Information* (Cambridge University Press, Cambridge, England, 2011).

[71] P. Talkner, E. Lutz, and P. Hänggi, Fluctuation theorems: Work is not an observable, Phys. Rev. E **75**, 050102(R) (2007).